(Received 1 July 2025, Accepted 1 September 2025, Scheduled 18 September 2025)

Structure-Preserving Discretization of the Magnetic Diffusion Equation Using DEC and FEEC

Lukas Schöppner* and Matthias Friedrich

Department of Electrical Engineering, University of Applied Science Fulda, Germany

ABSTRACT: This paper presents a numerical approach for solving the magnetic diffusion equation using structure-preserving discretization methods, like Discrete Exterior Calculus (DEC) and Finite Element Exterior Calculus (FEEC). A detailed derivation of DEC operators is provided, also their geometric foundation and relevance for discretizing differential forms on meshes. Furthermore, the paper includes an explicit introduction to the finite element exterior calculus framework, with a concise overview of the underlying functional spaces. The proposed formulations aim to preserve the topological and metric structure inherent in Maxwell's equation system. Numerical examples illustrate the stability and convergence of both methods, while also comparing their treatment of boundary conditions and discrete Hodge star construction which makes DEC and FEEC solvers spurious free and efficient useful for complex geometries.

1. INTRODUCTION

Numerical calculations of electromagnetic fields have become a crucial aspect in both academia and industry. The magnetic diffusion equation, which is a partial differential equation (PDE) and derived from the induction equation, is one of the fundamental concepts in Magnetohydrodynamics (MHD) and plays an important role in plasma physics. It explains how magnetic fields evolve over time due to the combined effects of fluid advection and resistive diffusion [1]. Moreover, ongoing research continues to explore stochastic effects and frequency-dependent behaviors, it provides a deeper insights into how the system evolves under different conditions [2]. In [4], using the magnetic diffusion equation for frequency domain calculation on a coaxial cable an asymptotic analysis of magnetic fields is presented for defining the *skin effect*, which is a consequence of the corresponding PDE solution. For a **B**-field analysis in the frequency domain, asymptotic expansions prove to be an ideal approach [3]. These expansions help to understand the behavior of magnetic fields, particularly in relation to the skin effect, which describes the tendency of alternating current to concentrate near the surface of a conductor at increasing frequencies. More important to say with the progressive development of quantum technology, incorporating quantum effects into computational electrodynamics has become increasingly important. One significant advantage of the **B**-field formulation is that it can be converted into an A-formalism, as the vector potential **A** provides a natural bridge between classical and quantum mechanical field theory. Thus, solutions of the diffusion equation with respect to quantum effects can also be considered without defining new formalisms. Such solutions are attributed to the quantum skin effect [5].

Exterior calculus is a mathematical framework from differential geometry that extends concepts from linear algebra in a more abstract way. This concept of differential forms was proposed by Cartan in 1899 [6]. Unlike traditional linear algebra, which primarily deals with scalars, vectors, and tensors, exterior calculus employs differential forms such as 0-forms, 1-forms, and 2-forms as representative quantities [7]. This approach allows for differentiation and integration over multidimensional manifolds, making exterior calculus particularly well-suited for applications of higher order dimensions. The first attempts to apply differential geometry in electrodynamics were made by Deschamps in 1981. He demonstrated that the physical dimensions of electromagnetic forms are structured in such a way that only two fundamental units are needed [8]. Discrete exterior calculus (DEC) can be described as a discrete smooth version of exterior calculus. The term DEC was first mentioned in 2003 by Hirani, who presented a discrete mathematical concept on a geometric and topological basis that allows integration and differentiation on cell complexes and its dual [9]. Further works on DEC in the field of computational electromagnetics (CEM) can be found in [29] and [30]. The mathematical framework of DEC extends exterior calculus notation by including operators such as the discrete Hodge star and discrete exterior derivative, while also generalizing the finite difference method (FDM). Unlike traditional numerical methods, DEC defines its operators purely through geometric properties, relying on the orientations of discrete elements such as rectangular or tetrahedral cells. Furthermore, these operators must satisfy fundamental mathematical principles, including generalized Stokes theorem and Poincaré's lemma. While DEC can be adapted to many types of mesh, like rectangular, tetrahedral or polygonial mesh shown in [10], FDM is only defined for rectangular mesh. Approaches to implement FDM on non-rectangular or unstructured meshes are defined by the approaches of conformal FDM [11] and curvilinear FDM [12]. In contrast, DEC offers much more flexibility in working with un-

* Corresponding author: Lukas Schöppner (lukas.schoeppner@et.hs-fulda.de).

structured or irregular meshes and handling with complex geometries. Another widely used numerical method in CEM is finite element method (FEM) [13]. Compared with DEC, FEM only uses primal mesh dicretization and is based on the weak formulation of PDEs, where the mass and stiffness matrices are derived using integral theorems [14]. In contrast, DEC is based on the exterior calculus formulation, utilizing differential forms and geometric operators. While FEM relies on basis functions and function spaces to approximate solutions [15], DEC discretizes differential forms directly on a mesh, making it well-suited for preserving the topological and geometric structure of underlying PDEs. Thus, using polynomials of the same order can lead to spurious solution, where charge conversation cannot necessarily be guaranteed in FEM [16]. When considering different polynomial degrees, various function spaces can be used, which are defined in the De Rham complex. The construction of these spaces, combined with exterior calculus, leads to Finite Element Exterior Calculus (FEEC) which was first introduced by Arnold [17]. FEEC utilizes the exterior calculus formulation in a way analogous to DEC which directly uses the exterior calculus-formulated PDE. Unlike standard FEM, FEEC not only is dependent on the orientation of the mesh but also incorporates the integral definitions of the finite element method. A key advantage of FEEC over FEM is that the polynomial degree is naturally determined by the De Rham complex [18]. This prevents spurious solutions in CEM, whereas FEM heavily uses basis function interpolation, which can be less effective in preserving geometric consistency on nonuniform meshes. The incorporation of primal and dual structures, along with the consideration of topology, geometry, and polynomial spaces, makes DEC and FEEC efficient solvers for numerical methods. The aim of this work is to present a detailed approach using DEC and FEEC to solve the magnetic diffusion equation in two dimensions. The paper is structured as follows. Section 2 presents an explicit derivation of the magnetic diffusion equation. The exterior calculus formulation of this equation, along with the relevant operators, is introduced in Section 3. Section 4 provides a detailed explanation of the DEC approach, including its geometrically defined operators. The derivation and implementation of FEEC, along with its corresponding operators, are discussed in Section 5. Section 6 covers the implementation and numerical simulations of both methods. Finally, a conclusion of this work is summarized in Section 7.

2. MAGNETIC DIFFUSION EQUATION

The well-known magnetic diffusion equation is a simplification of the induction equation from magnetohydrodynamics (MHD) [19]. From Maxwell's equation system, we start with Ampere-Maxwell law using quasistatic approximation and Faraday Law.

$$\nabla \times \mathbf{B} = \mu_0 \mathbf{J} \tag{1}$$

$$\nabla \times \mathbf{E} = -\frac{\partial \mathbf{B}}{\partial t} \tag{2}$$

whereby $\mathbf{E}$ is the electric field, $\mathbf{B}$ the magnetic flux density, $\mathbf{J}$ the current density, and μ_0 the permeability. $\mathbf{J}$ can also be expressed by Ohm's law

$$\mathbf{J} = \sigma \left(\mathbf{E} + \mathbf{v} \times \mathbf{B} \right) \tag{3}$$

here the vector $\mathbf{v}$ describes the velocity of a moving reference frame, and σ is the electrical conductivity.

Inserting $\mathbf{J}$ in (1) and applying the curl operator to both sides, the following equation has the form

$$\nabla \times \mathbf{E} = \frac{1}{\mu_0 \sigma} \nabla \times (\nabla \times \mathbf{B}) - \nabla \times (\mathbf{v} \times \mathbf{B}) \tag{4}$$

Using the curl identity

$$\nabla \times (\nabla \times \mathbf{B}) = \nabla(\nabla \cdot \mathbf{B}) - \nabla^2 \mathbf{B} \tag{5}$$

combined with the non-monopole law

$$\nabla \cdot \mathbf{B} = 0 \tag{6}$$

the expression (4) gives

$$\frac{\partial \mathbf{B}}{\partial t} - \frac{1}{\mu_0 \sigma} \nabla^2 \mathbf{B} - \nabla \times (\mathbf{v} \times \mathbf{B}) = 0 \tag{7}$$

Equation (7) is called *induction equation* and widely used in MHD for relating velocity and magnetic fields with electrically conductive fluids [20]. In engineering, a geometry is usually considered in a rest frame with $\mathbf{v} = 0$, whereby Equation (7) is thus simplified to the *magnetic diffusion equation* [21]

$$\frac{\partial \mathbf{B}}{\partial t} - \frac{1}{\mu_0 \sigma} \nabla^2 \mathbf{B} = 0 \tag{8}$$

In the frequency domain, the magnetic diffusion equation is reformulated by applying the Fourier transform, which simplifies first time derivatives to $i\omega$ and leads to

$$i\omega \mathbf{B} - \frac{1}{\mu_0 \sigma} \nabla^2 \mathbf{B} = 0 \tag{9}$$

3. EXTERIOR CALCULUS FRAMEWORK

Physical quantities can be expressed in the language of differential forms using the framework of exterior calculus. To describe (9) in terms of differential forms, $\mathcal{B}$ is denoted as a 2-form.

$$\mathcal{B} = d(\mathbf{A}^\flat) = d\mathcal{A} \tag{10}$$

The flat operator $\flat$ is a mapping from vector potential fields $\mathbf{A}$ to potential 1-forms $\mathcal{A}$.

The Laplace operator ∇^2 is rewritten using the Laplace De Rham operator [22]

$$\nabla^2 = \delta d + d\delta \tag{11}$$

This is a composition of the exterior derivative d and the codifferential δ. The exterior derivative maps a p-form to a $(p+1)$-form. The codifferential is a combination of d and Hodge Star operator $\star$

$$\delta = (-1)^{n(p+1)+1+s} \star d \star \tag{12}$$

and maps a p-form to a $(p-1)$-form. δ depends on the form p used for the exterior formulation, dimension n, and signature

s of the manifold. For most geometric problems in electrodynamics, the dimension of the manifold represents the dimension of the space $\mathbb{R}^n$. One assigned an $s = 0$ to such manifolds [23], and δ can be simplified.

$$\delta = (-1)^{n(p+1)+1} \star d \star \tag{13}$$

The Hodge Star operator acts also on arbitrary p-forms and maps them to $(n-p)$-forms. A fundamental treatment of differential forms and their operators is provided in [24]. For more information on manifolds and their signatures, see [25, 26].

By using the definition given in (11), Equation (9) can be reformulated in the language of differential forms.

$$i\omega\mathcal{B} - \frac{1}{\mu_0\sigma}(\delta d + d\delta)\mathcal{B} = 0 \tag{14}$$

For the two dimensional case $n = 2$, (14) is reduced to

$$i\omega\mathcal{B} + \frac{1}{\mu_0\sigma}(d \star d\star)\mathcal{B} = 0 \tag{15}$$

since the exterior derivative of a 2-form in two dimensions always vanishes, the first term in (11) does not contribute. The magnetic diffusion equation in a formulation of the potential 1-form results from the substitution of $\mathcal{B}$ by (10).

$$i\omega\, d\mathcal{A} + \frac{1}{\mu_0\sigma}(d \star d \star d)\mathcal{A} = 0 \tag{16}$$

A formulation of the magnetic diffusion equation in terms of the vector potential $\mathbf{A}$ introduces additional complexity and requires specific assumptions about the field, such as the choice of a gauge condition (e.g., the Coulomb gauge $\nabla \cdot \mathbf{A} = 0$) [27]. In contrast, the exterior calculus formulation naturally expresses $\mathcal{B}$ as $d\mathcal{A}$, eliminating the need for gauge conditions and reducing computational overhead. Therefore, Equation (15) will be used in the following sections.

4. MAGNETIC DIFFUSION IN DISCRETE EXTERIOR CALCULUS NOTATION

The idea of a discrete version of the formalism presented in Section 3 was firstly introduced by Whitney who developed a systematic way to discretize differential forms on simplicial complexes [28] and established an isomorphism between differential forms and simplicial cochains [29].

A *simplicial complex* $\mathcal{K}$ is a oriented collection of all simplices σ^n that approximates a given geometry in $\mathbb{R}^n$ [30]. Mathematically, a simplicial complex can be defined as

$$\mathcal{K} = \left[\sigma^1, \sigma^2, \ldots, \sigma^n\right] \tag{17}$$

where each n-simplex σ^n is expressed by an oriented set of $(n+1)$ vertices v_i [31] as seen in Figure 1.

$$\sigma^n = \{v_1, v_2, \ldots, v_{n+1}\} \tag{18}$$

The simplices are typically arranged to form a triangulated or meshed representation such as tetrahedral or rectangular meshes of the underlying geometry.

In the context of simplicial complexes, the discrete formulation of a differential form is represented by a *simplicial cochain*.

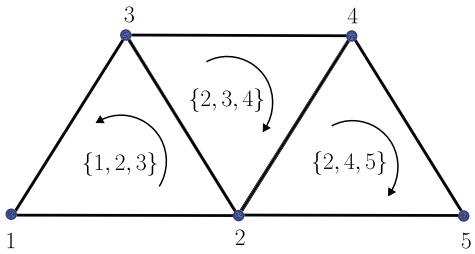

FIGURE 1. Three simplices in a two dimensional space with defined vertices and orientation.

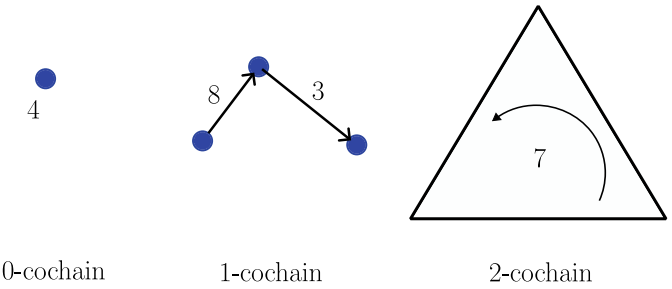

FIGURE 2. Illustration of three different cochains each assigned a scalar value as an example.

A simplicial cochain assigns a scalar value to each n-simplex in the complex $\mathcal{K}$ [32]. For instance, a 0-cochain assigns a scalar value to each vertex (see Figure 2), similar to how functions correspond to 0-forms, while a 1-cochain assigns scalar values to edges, analogous to assigning values to 1-forms.

The discrete exterior derivative defined on primal p-cochains are represented by matrices that acts on the respective cochain in DEC, namely $\mathbf{d}^{(0)}$, $\mathbf{d}^{(1)}$ for the two-dimensional case. The superscript indicates that the operator acting on the given cochain—such as (0)—operates on primal 0-cochains. The elements of $\mathbf{d}^{(0)}$ can assume three different values depending on the orientation.

$$\left[\mathbf{d}^{(0)}\right]_{i,j} = \begin{cases} 1 & \text{if } v_i \text{ is on } l_i \text{ with normal orientation,} \\ -1 & \text{if } v_i \text{ is on } l_i \text{ with flipped orientation,} \\ 0 & \text{else} \end{cases} \tag{19}$$

and has the dimension $N_E \times N_V$, where N_V is the number of vertices v_i and N_E the number of edges l_i of a discretized geometry. The number of primal faces S_i is denoted as N_F. Similar to (19), $\mathbf{d}^{(1)}$ operates on primal 1-cochains and has the dimension $N_F \times N_E$. Generally $\mathbf{d}^{(k)}$ acts on p-cochains and returns a $(p+1)$-cochain.

$$\left[\mathbf{d}^{(1)}\right]_{i,j} = \begin{cases} 1 & \text{if } l_i \text{ is on } S_i \text{ with normal orientation,} \\ -1 & \text{if } l_i \text{ is on } S_i \text{ with flipped orientation,} \\ 0 & \text{else} \end{cases} \tag{20}$$

The discrete exterior derivative can also be constructed in the dual space by considering the relationships between dual vertices, dual edges, and dual faces as shown in Figure 3.

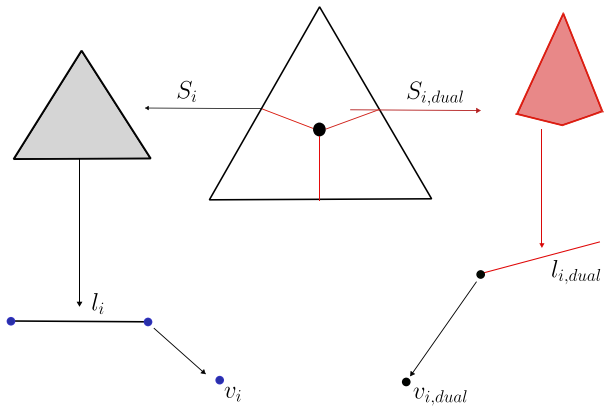

FIGURE 3. Illustration of a 2D simplex with primal and dual meshes, highlighting the respective assignment of primal and dual faces S, edges l and vertices v.

Due to the geometric duality between the primal and dual meshes, the following relation holds [33]:

$$\mathbf{d}_{dual}^{(n-p)} = (-1)^p \left(\mathbf{d}^{(p-1)}\right)^T \tag{21}$$

n is the dimension and p the cochain information. In 2D case $n = 2$, the dual operators are

$$\mathbf{d}_{dual}^{(0)} = \left(\mathbf{d}^{(1)}\right)^T \tag{22}$$

and

$$\mathbf{d}_{dual}^{(1)} = -\left(\mathbf{d}^{(0)}\right)^T \tag{23}$$

A key property of the discrete exterior derivative is its purely topological nature, meaning that it does not depend on the geometry of the given manifold, i.e., the metric. Furthermore, it satisfies the *Poincaré Lemma*, implying that applying the discrete exterior derivative twice yields zero.

$$\mathbf{d}^{(p)} \cdot \mathbf{d}^{(p-1)} = \mathbf{0} \tag{24}$$

In DEC, the Hodge star operator $\star$ defines a mapping between the cochains of the primal and dual complexes. To construct the Hodge Star, the circumcentric dual mesh is commonly used, which is orthogonal to the primal mesh [34]. This dual mesh enables the Hodge star operator to be represented as a diagonal sparse matrix, encoding the relationships between primal and dual simplices.

The relationships between the primal and dual simplices are described by the dual simplex $\sigma_i^{\star(n-p)}$ and the primal simplex $\sigma_i^{(p)}$. These simplices are geometrically interconnected, and the Hodge star operator captures the duality of forms between the primal and dual complexes [35]. In practice, the Hodge star is represented by a matrix whose diagonal and off-diagonal elements are based on the area- and length-based relationships between the primal and dual mesh. Mathematically, it is formulated as

$$\star_{ii}^{(p)} = \frac{|\sigma_i^{\star(n-p)}|}{|\sigma_i^{(p)}|} \tag{25}$$

For each primal simplex $\sigma_i^{(p)}$, the corresponding dual simplex $\sigma_i^{\star(n-p)}$ is determined using geometric quantities such as area or length which are defined as $|\sigma|$ in (25) depending on the corresponding p-cochain.

In two dimensions, we can calculate three different Hodge stars: The Hodge star acting on a 0-primal cochain is given by

$$\star_{ii}^{(0)} = vol\left(\sigma_i^{\star(2)}\right) \tag{26}$$

where vol is the area of the dual cells. The Hodge star acting on a 1-primal cochain is expressed as

$$\star_{ii}^{(1)} = \frac{|\sigma_i^{\star(1)}|}{|\sigma_i^{(1)}|} \tag{27}$$

which relates the length of the dual edges to the length of the primal edge. Finally, the Hodge star acting on 2-primal cochains is defined as

$$\star_{ii}^{(2)} = \frac{1}{vol\left(\sigma_i^{(2)}\right)} \tag{28}$$

Here, $vol(\sigma_i^{(2)})$ represents area of the primal simplices.

The relationship between the primal complex and dual cell complex can be interpreted through the framework of the De Rham complex shown in Figure 4.

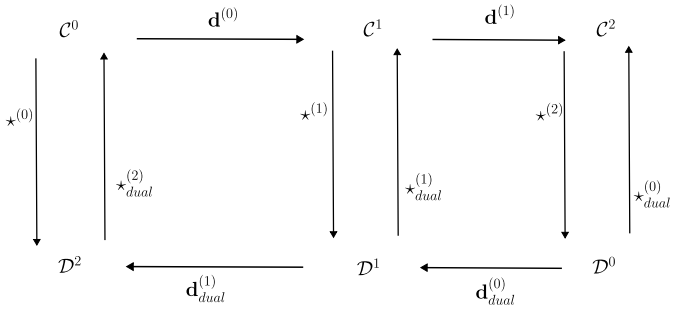

FIGURE 4. De Rham complex in the 2D case where $\mathcal{C}^n$ denotes the space of all primal n-cochains while $\mathcal{D}^n$ represents dual n-cochains. The complex highlights the interplay between primal and dual structure also between the cochains though the discrete exterior derivative $\mathbf{d}^{(n)}$ and its dual $\mathbf{d}_{dual}^{(n)}$.

In the case of a circumcenter-based dual mesh, the Hodge star operator acting on the primal mesh is related to the dual Hodge star $\star_{dual}^{(p)}$ by an inverse relationship of the Hodge star defined on the primal mesh using the relationship [36]

$$\star_{ii,dual}^{(p)} = \left(\star_{ii}^{(n-p)}\right)^{-1} \tag{29}$$

This inverse property holds the diagonal structure of the resulting Hodge matrices. As a consequence, the circumcentric dual approach allows for a straightforward computation of the Hodge star, ensuring numerical efficiency while preserving the geometric consistency.

To discretize the magnetic diffusion Equation (9) in DEC notation, the exterior calculus formulation from (15) is employed,

TABLE 1. Illustration of element types from the Finite Element Method in relation to the function space in 2D.

Properties	H^1	$H(\text{curl})$	$H(\text{div})$	L^2
Illustration				
FE-Element Types	-Lagrange -Crouzeix-Raviart	-Nedelec rst kind, -Nedelec seconnd kind	-Raviart-Thomas, -Brezzi-Douglas -Madral-Tai-Winter	-Discontinous Lagrange
Ref.	[37]	[37], [38]	[37], [39]	[37], [40]

utilizing the appropriate operators adapted to both the primal and dual meshes.

$$i\omega B + \frac{1}{\mu_0 \sigma}\left(\mathbf{d}^{(1)}\ (\star^{(1)})^{-1}\ (\mathbf{d}^{(1)})^T\ \star^{(2)}\right) B = 0 \tag{30}$$

Since $\mathcal{B}$ is a 2-form in the cochain representation of differential forms, its DEC representation is obtained from the surface integral of B along each surface S_i. This integral is expressed as

$$B_i = \int_{S_i} B \cdot \mathbf{n}\, \mathrm{d}S \tag{31}$$

Thus, the vector B which includes the integral of each surface on the primal mesh is an $(N_F \times 1)$ vector defined as

$$B = [B_1, B_2, B_3, \ldots, B_{N_F}]^T \tag{32}$$

Therefore, the unknown components of the 2-cochain B are defined in (32) which includes the magnetic flux on each S_i.

5. FINITE ELEMENT EXTERIOR CALCULUS FORMULATION

The exterior calculus can be integrated with the finite element method through the framework of *finite element exterior calculus* (FEEC). This approach leverages the De Rham complex within the context of finite element analysis [41]. FEM provides different solution strategies depending on the problem at hand, with the choice of appropriate finite elements playing a crucial role. A common selection is Lagrange elements, where nodal values are associated with each element. In electrodynamics, partial differential equations (PDEs) often involve vector-valued solutions. To account for the specific characteristics of vector fields, such as curl and divergence-free properties, edge elements are typically employed for getting accurate representation of these field characteristics [42].

The classical FEM employs Lagrange elements, using interpolation polynomials ϕ_i that come from a certain function space, the *Sobolev space* [44]. The condition imposed by this function space is that the integral of the absolute value square of the interpolation polynomial used (linear or quadratic) is finite. If this is true, the polynomial ϕ_i is L^2-*integrable* over the given meshed geometry Ω.

$$L^2(\Omega) = \left(\phi_i \ ; \sqrt{\int_\Omega |\phi_i|^2\, d\Omega} < \infty\right) \tag{33}$$

Interpolation functions that fulfill property (33) are elements of the so called function space H^1 [43]. It is important to note that the derivative of ϕ is also in L^2.

$$H^1 = \{\ \phi \in L^2\ \mid \nabla\phi \in [L^2]^3\} \tag{34}$$

The bracket term $[L^2]^3$ describes the components of $\nabla\phi$ in 3D. For 2D case, the notation $[L^2]^2$ is used.

In the case of edge elements, a distinction is made between elements, which are intended to take account of curl and divergence properties in the calculations. Vector functions $\mathbf{v}$ are used, which are located in $H(\text{curl})$ with the property

$$H(\text{curl}) = \{\ \mathbf{v} \in L^2\ \mid \nabla \times \mathbf{v} \in [L^2]^3\} \tag{35}$$

and $H(\text{div})$

$$H(\text{div}) = \{\ \mathbf{v} \in L^2\ \mid \nabla \cdot \mathbf{v} \in L^2\} \tag{36}$$

respectively. Using these properties, the De Rham Complex of the finite element method for a given Ω in 2D is represented as follows

$$H^1(\Omega) \xrightarrow{\text{grad}} H(\text{curl}, \Omega)/H(\text{div}, \Omega) \xrightarrow{\text{curl/div}} L^2(\Omega) \tag{37}$$

A graphical overview of individual elements with their characteristics and examples of elements that are typically used for the respective functional space are shown in Table 1.

The concept of FEEC like DEC is based on the discrete De Rham complex as shown in Figure 4. The difference lies in the construction of the operators. While DEC constructs the Hodge stars and discrete exterior derivatives using geometric interpretation, FEEC uses the basis function approach using integral representation for the operators. The mapping from a primal cochain to a dual one in FEEC is constructed using the defini-

tion of mass matrix $\mathbb{M}_{i,j}^{(n)}$ over the element T

$$\mathbb{M}_{i,j}^{(n)} = \int_T \varphi_i \cdot \varphi_j \, dS \tag{38}$$

whereby φ are the elements of the given primal n-cochains. $\mathbb{M}_{i,j}$ serves as the discrete analogue of the Hodge star operator from DEC. However, although the Hodge star is defined using circumcentric dual meshes, the computations in FEEC are based on barycentric dual as seen in Figure 5, ensuring compatibility with finite element function spaces.

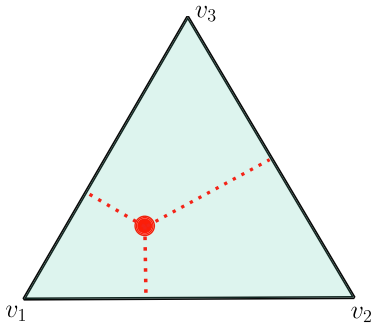

FIGURE 5. Illustration of a dual 0-form on a cell which is barycentric on the triangle.

A suitable assignment of the given functional spaces in the discrete De Rham complex can be constructed using (48). The functions in H^1 are the primal 0-cochain, and functions from $H(\text{curl})/H(\text{div})$ in 2D represent the mass matrix for the primal 1-cochain and L^2-elements in (38) for φ represent the mass matrix for the primal 2-cochain.

The discrete exterior derivative $\mathbb{D}$ in FEEC has the same geometric interpretation as in DEC, a mapping from a p-cochain to a $(p+1)$-cochain. So $\mathbb{D}^{(0)}$ acts on primal 0-cochains and $\mathbb{D}^{(1)}$ on primal 1-cochains. For $\mathbb{D}^{(0)}$, the matrix representation follows from the integral

$$\mathbb{D}_{i,j}^{(0)} = \int_T \eta_i \cdot \text{grad}(\phi_j) \, dS \tag{39}$$

whereby η_i are $H(\text{curl})$-elements representing the primal 1-cochain in (39). The same procedure applies to $H(\text{div})$ elements.

Accordingly, $\mathbb{D}^{(1)}$ is also calculated by the use of [34]

$$\mathbb{D}_{i,j}^{(1)} = \int_T w_i \cdot \text{curl}(\eta_j^{H(\text{curl})}) \, dS \tag{40}$$

whereby w_i are L^2-elements. For $H(\text{div})$, the divergence operator must be used for the element

$$\mathbb{D}_{i,j}^{(1)} = \int_T w_i \cdot \text{div}(\eta_j^{H(\text{div})}) \, dS \tag{41}$$

The $\mathbb{D}$-operators must also satisfy the condition (24)

$$\mathbb{D}^{(p)} \cdot \mathbb{D}^{(p-1)} = \mathbf{0} \tag{42}$$

The dual discrete exterior derivative can also be calculated by using (21)

$$\mathbb{D}_{dual}^{(n-p)} = (-1)^p \, (\mathbb{D}^{(p-1)})^T \tag{43}$$

whereby the relation of the dual and primal mesh as in DEC is maintained.

5.1. FEEC Approach for the Magnetic Diffusion Equation

In the 2D case of the magnetic diffusion equation, it is crucial to determine the appropriate mass matrix $\mathbb{M}^{(1)}$, since there are two possibilities as seen in (48).

To determine the 1-cochain mass matrix, a weak formulation of (9) is defined by using the identity $\nabla^2 = -\nabla \times \nabla \times$ and the corresponding test function $\mathbf{w}$

$$\int_S i\omega \mathbf{B} \cdot \mathbf{w} \, dS + \frac{1}{\mu_0 \sigma} \int_S \nabla \times (\nabla \times \mathbf{B}) \cdot \mathbf{w} \, dS = 0 \tag{44}$$

With the application of the Stoke theorem and vector identity

$$(\nabla \times \nabla \times \mathbf{B}) \cdot \mathbf{w} = (\nabla \times \mathbf{B}) \cdot (\nabla \times \mathbf{w}) - \nabla \cdot (\mathbf{w} \times (\nabla \times \mathbf{B})) \tag{45}$$

the second integral can be reformulated as

$$\begin{aligned} &\int_S \nabla \times (\nabla \times \mathbf{B}) \cdot \mathbf{w} \, dS \\ &= \int_S (\nabla \times \mathbf{B}) \cdot (\nabla \times \mathbf{w}) \, dS - \int_S \nabla \cdot [\mathbf{w} \times (\nabla \times \mathbf{B})] \, dS \\ &= \int_S (\nabla \times \mathbf{B}) \cdot (\nabla \times \mathbf{w}) \, dS - \oint_{\partial S} \mathbf{w} \times (\nabla \times \mathbf{B}) \, dl \end{aligned} \tag{46}$$

The second term in (46) describes the implementation for Neumann boundary conditions [45]. In the first term, it is straightforward to see that $\mathbf{w}$ needs to be defined in the $H(\text{curl})$-space compared to the defined property in (35).

By continuing the FEM approach, the mass matrix is determined using the Galerkin approach for (44) and the approximation for the magnetic field $B_i \approx \sum_{i=1}^{n} b_i N_i$.

$$\begin{aligned} &i\omega \sum_{i=1}^{n} b_i \int_S N_i \cdot N_j \, dS \\ &+ \frac{\sum_{i=1}^{n} b_i}{\mu_0 \sigma} \int_S (\nabla \times N_i) \cdot (\nabla \times N_j) \, dS = 0 \end{aligned} \tag{47}$$

where N_i, N_j are the basis functions. In Equation (47), the first term represents the mass matrix, while the second term corresponds to the stiffness matrix. Since the basis functions have

a rotational property, our basis functions must be in $H(\text{curl})$, which defines the 2D De Rham complex.

$$H^1(\Omega) \xrightarrow{\text{grad}} H(\text{curl}, \Omega) \xrightarrow{\text{curl}} L^2(\Omega) \tag{48}$$

For our FEEC approach, only the mass matrix is required. To ensure conformity with the function space $H(\text{curl})$, we employ Nédélec elements of the first kind as the basis N_i, denoted as η_i^{Ned} for the construction of the mass matrix $\mathbb{M}_{i,j}^{(1)}$.

$$\mathbb{M}_{i,j}^{(1)} = \int_S \eta_i^{\text{Ned}} \cdot \eta_j^{\text{Ned}} \, dS \tag{49}$$

A mathematically detailed description of Nédélec elements, including their mapping properties, can be found in [46, 47]. The FEEC formulation of the magnetic diffusion equation is equivalent to the DEC approach. Here, only $\star$ is replaced by $\mathbb{M}$ and $\mathbf{d}$ by $\mathbb{D}$. The FEEC formulation of the magnetic diffusion equation is equivalent to the DEC approach. In this framework, the operator $\star_{i,j}^{(n)}$ is replaced by the mass matrix $\mathbb{M}_{i,j}^{(n)}$, while the exterior derivative $\mathbf{d}_{i,j}^{(n)}$ corresponds to the discrete operator $\mathbb{D}_{i,j}^{(n)}$.

$$i\omega B + \frac{1}{\mu_0 \sigma} \left(\mathbb{D}^{(1)} \left(\mathbb{M}^{(1)} \right)^{-1} \left(\mathbb{D}^{(1)} \right)^T \mathbb{M}^{(2)} \right) B = 0 \tag{50}$$

Here, $\mathbb{M}^{(2)}$ is defined in the same way as $\star^{(2)}$ in (28) and represents a diagonal matrix.

$$\mathbb{M}_{i,i}^{(2)} = \star_{i,i}^{(2)} \tag{51}$$

This approach is only valid by using the lowest order elements like Nedelec first kind, so the elements w_i in L^2 are piecewise cell-based constant. However, despite its simplicity, this ansatz is not generally applicable. When higher-order finite elements are used like higher order polynomials, the cellwise basis functions w_i in L^2 are no longer constant but instead exhibit polynomial variations within the element. The curl components of the lowest-order Nédélec elements is constant, which justifies the approximation of L^2-space elements as constant. However, for higher-order Nédélec elements, the components of the curl are no longer linear in L^2, meaning that L^2-space elements can no longer be accurately approximated using constant elements. As a result, the mass matrix involves integrals of nontrivial functions, making a simple area-based scaling insufficient. Detailed information on the dependence of the functional space and polynomial degree are found in [16] and [18].

Finally, the matrix $\mathbb{D}^{(1)}$ can be constructed using

$$\mathbb{D}_{i,j}^{(1)} = \int_T w_i \cdot \text{curl}(\eta_j^{\text{Ned}}) \, dS \tag{52}$$

It should be noted that, unlike the Hodge star $\star_{i,i}^{(1)}$, the mass matrix $\mathbb{M}_{i,j}^{(1)}$ is no longer a diagonal matrix because the entries involve integrals of overlapping basis functions η_i^{Ned}, leading to a more general sparse structure.

6. IMPLEMENTATION AND NUMERICAL RESULTS

The implementation of the magnetic diffusion equation in DEC and FEEC was simulated using a copper disk with radius $r = 2\,\text{mm}$ shown in Figure 6. This problem is defined with Dirichlet boundary conditions ∂B, so that a fixed **B**-field is given at the edge of the geometry.

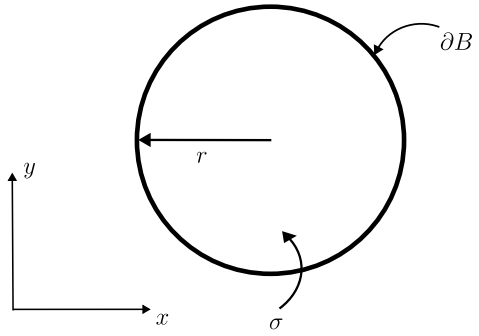

FIGURE 6. Illustration of the disk with assignment of the boundary condition of the geometry as well as the copper conductivity coefficient σ.

The implementation of the boundary conditions is crucial, since we have a 2-cochain B here, so we have to define the boundary conditions with $I = 1A$

$$\partial B = \frac{I}{2\pi\mu_0 r} \tag{53}$$

for both implementing methods on the *surfaces* at the boundary. Since B represents a primal 2-cochain, its Dirichlet boundary conditions are surface elements defined by the boundary nodes. In Figure 8, a simple example is shown. By definition, B is associated with the faces of the primal mesh and is given by the integral of the underlying vector field through each face Ω. For boundary conditions, the face areas on the boundary must be extracted.

$$\begin{aligned} \oint_\Omega \mathbf{B} \cdot \mathbf{n} \, dS &= \sum_{S \in \Omega} \int \mathbf{B} \cdot \mathbf{n} \, dS \\ &= B_{S_1} + B_{S_2} + B_{S_3} + B_{S_4} + B_{S_5} \end{aligned} \tag{54}$$

Here, the values B_{S_i} are the integral of **B** along the defined area S_1. These areas are defined over extracted points p_i

$$\begin{aligned} &B_{S_1} + B_{S_2} + B_{S_3} + B_{S_4} + B_{S_5} \\ &= B_{\overline{p_1 p_2 p_3}} + B_{\overline{p_2 p_4 p_3}} + B_{\overline{p_3 p_4 p_5}} + B_{\overline{p_4 p_6 p_5}} + B_{\overline{p_5 p_6 p_7}} \end{aligned} \tag{55}$$

For our discretized problem, the primal 2-cochain naturally associates the vector field with surface elements, and Dirichlet boundary conditions are applied on the corresponding boundary faces. In exterior calculus, boundary conditions are not universal but depend on the geometry and discretization. It can be seen that the implementation of the boundary condition can be carried out independently of any integral theorems, relying solely on the n-cochain associated with the solution variable. By applying the Stokes-Cartan theorem, the integral formulation becomes purely topological, even for divergence-type problems of B, where Dirichlet boundary conditions correspond to boundary face elements and are independent of the

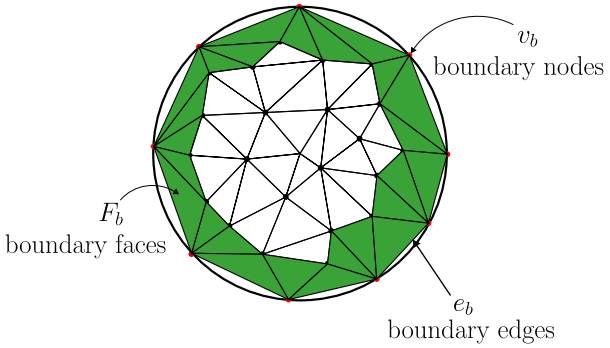

FIGURE 7. Delaunay unstructured meshed geometry with boundary nodes v_b, edges e_b and faces F_b.

geometric structure of the domain.

$$\int_V dB = \int_{\partial V} B \tag{56}$$

The geometric properties for a curl problem of the domain are no longer contained in the integrand itself but are entirely encoded in the Hodge star operator.

$$\int_S d \star B = \int_{\partial S} \star B \tag{57}$$

To determine the size of each boundary, the corresponding boundary nodes v_b must first be identified. A boundary edge e_b is classified as an edge if it is exclusively defined by two edge nodes. Furthermore, any face that contains at least one edge node is considered a boundary face F_b. An illustrative example is shown in Figure 7. When extracting the indices of v_b, e_b, F_b they must be inserted into the respective matrices to solve the DEC formulation within the FEEC framework. Taking the exterior derivative $\mathbf{d}^{(1)}$ from DEC as an example, the matrix needs to be modified to incorporate boundary conditions. Specifically, all boundary edge indices and boundary face indices must be removed from $\mathbf{d}^{(1)}$ to ensure that only the inner boundaries of B are considered by the system of equations. Conversely, the corresponding $\mathbf{d}^{(1)}$ operator for the boundary retains all indices of e_b and F_b. The same procedure is applied to the matrix $\mathbb{D}^{(1)}$, as it has the same dimensions and follows the same structural modifications. In addition to modifying the exterior derivative matrices, the Hodge star operators must also be adjusted to properly account for the boundary conditions. For example, when constructing the $\star^{(2)}$, only the indices corresponding to interior faces are considered to determine the correct size of B. In contrast, the indices associated with F_b are included in a separate Hodge operator that incorporates the boundary conditions. Similarly, the Hodge $\star^{(1)}$ must be adapted so that it correctly reflects the influence of boundary edges. Once these modifications have been made, the same procedure is applied to the mass matrices $\mathbb{M}^{(1)}$ and $\mathbb{M}^{(2)}$ to ensure consistency throughout the formulation.

This implementation transforms, in the DEC case, (30) in two parts due to the separation of $B = B_{sol} + B_{bdy}$. Matrix B_{bdy} represents the boundary conditions, i.e., $B_{bdy} = \partial B$,

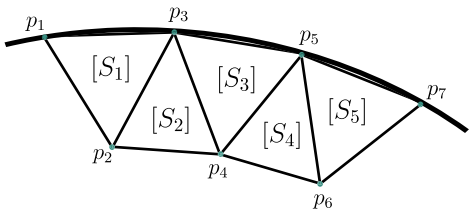

FIGURE 8. Dirichlet boundary of a primal 2-cochain.

while B_{sol} corresponds to the desired solution quantity.

$$\left[i\omega + \frac{1}{\mu_0 \sigma}\left(\mathbf{d}^{(1)}\,(\star^{(1)})^{-1}\,(\mathbf{d}^{(1)})^T\,\star^{(2)}\right)\right] B_{sol}$$
$$+ \left[i\omega + \frac{1}{\mu_0 \sigma}\left(\mathbf{d}^{(1)}\,(\star^{(1)})^{-1}\,(\mathbf{d}^{(1)})^T\,\star^{(2)}\right)\right] B_{bdy} = 0 \tag{58}$$

The matrices contained in the first bracket are the revised matrices in which the indices of v_b, e_b, and F_b have been removed. These indices have been assigned to the second bracket, which refers specifically to the Dirichlet boundary condition (53) to the corresponding F_b. The FEEC matrix system from (50) can also be transformed following Equation (58) and adheres to the same approach regarding the separation of matrices based on boundary indices and interior indices.

$$\left[i\omega + \frac{1}{\mu_0 \sigma}\left(\mathbb{D}^{(1)}\,(\mathbb{M}^{(1)})^{-1}\,(\mathbb{D}^{(1)})^T\,\mathbb{M}^{(2)}\right)\right] B_{sol}$$
$$+ \left[i\omega + \frac{1}{\mu_0 \sigma}\left(\mathbb{D}^{(1)}(\mathbb{M}^{(1)})^{-1}(\mathbb{D}^{(1)})^T\mathbb{M}^{(2)}\right)\right] B_{bdy} = 0 \tag{59}$$

This ensures a consistent treatment of boundary conditions across the formulation. It is important to note that matrix iw is always adapted to the size of the respective modified matrix complex in order to keep the calculations consistent.

To determine B_{sol}, it is necessary to compute the inverse of the first bracket term from Equations (58) in DEC and (59) for FEEC. Since these matrices are typically sparse, it is beneficial to use sparse approximate inverse techniques (SPAI), which allow for efficient computation while preserving sparsity. These techniques are particularly useful in large-scale problems, where directly computing the full inverse would be computationally expensive and memory-intensive [48, 49]. Another possible approach is to use the Moore-Penrose pseudoinverse, which is well-suited for calculation of the inverse for non-square matrices. However, this method has limitations when being applied to sparse matrices, as it requires converting the matrix into a dense format before computing the inverse [50].

In Figure 9, the solution of the magnetic diffusion equation within the DEC formalism is presented, and the FEEC solution is shown in Figure 10. Both results illustrate how the magnitude of the magnetic field distribution changes with increasing frequency. Specifically, as the frequency increases, the magnetic field strength within the conductor decreases which is due to the skin effect. The four different cases in the figure clearly show this effect, with the field becoming weaker inside the conductor as the frequency increases.

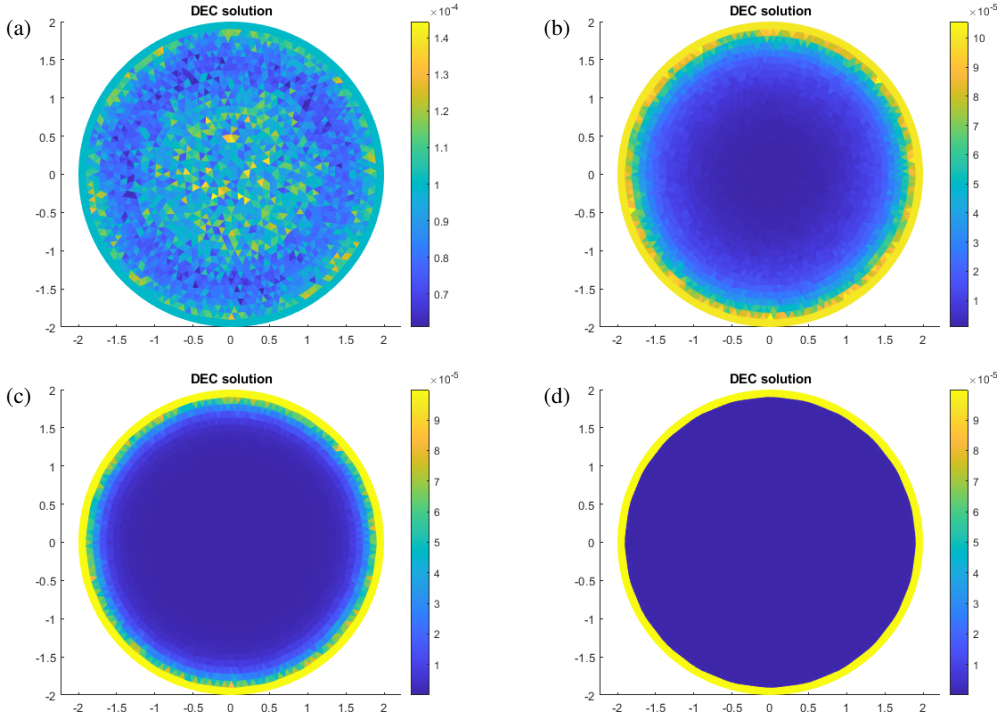

FIGURE 9. The calculation of the magnitude for B in DEC formulation was performed for different frequencies: (a) $f = 50\,\text{Hz}$, (b) $f = 5\,\text{kHz}$, (c) $f = 20\,\text{kHz}$, and (d) $f = 5\,\text{MHz}$.

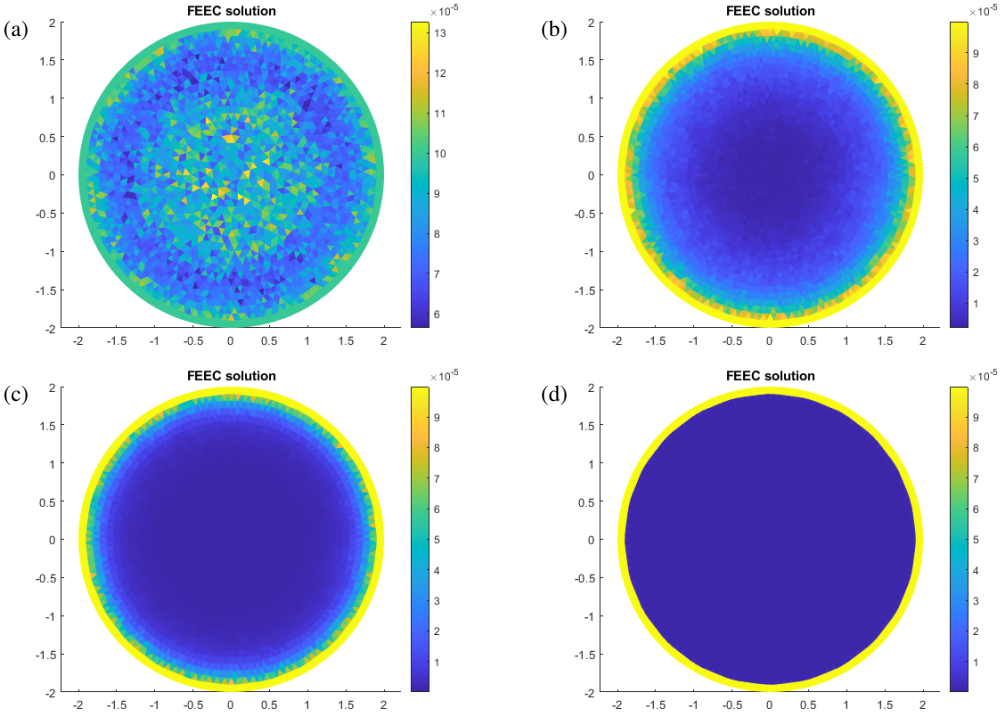

FIGURE 10. FEEC solution for the magnitude of B for different frequency values: (a) $f = 50\,\text{Hz}$, (b) $f = 5\,\text{kHz}$, (c) $f = 20\,\text{kHz}$, and (d) $f = 5\,\text{MHz}$.

The analytical solution B_{an} of Equation (9), based on modified Bessel functions, was taken from [21]. Under the given boundary conditions, it yields to

$$B_{an} = B_0 \frac{J_0(\gamma, r)}{J_0(\gamma, r_0)} \tag{60}$$

B_0 incorporates the boundary conditions from (53), while J_0, being modified Bessel functions of the first kind, are used for describing the behavior at the boundary $r_0 = 2\,\text{mm}$ and for all values of r in the range $0 < r < r_0$. Parameter γ contains a square root term involving a problem-specific constant

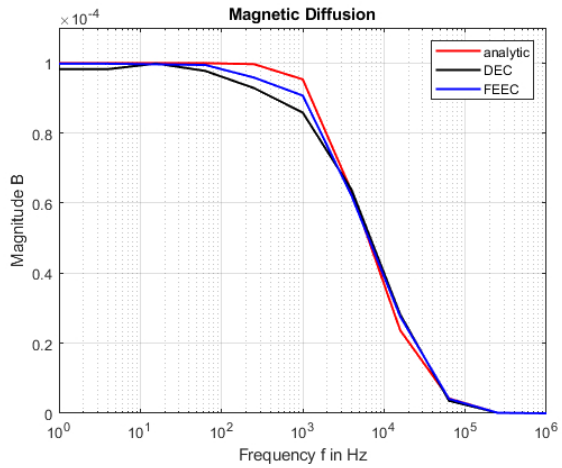

FIGURE 11. Illustration of the numerical results obtained with FEEC and DEC methods in comparison with the analytical solution at the radial position $r = 1.1$ mm in the domain.

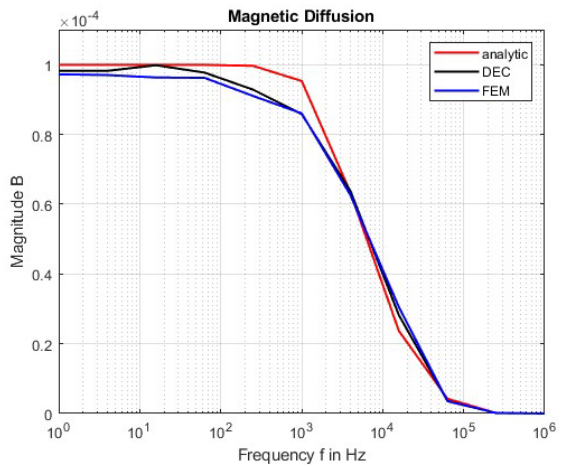

FIGURE 12. Numerical results illustrating the comparison of DEC with FEM solutions at the radial position $r = 1.1$ mm.

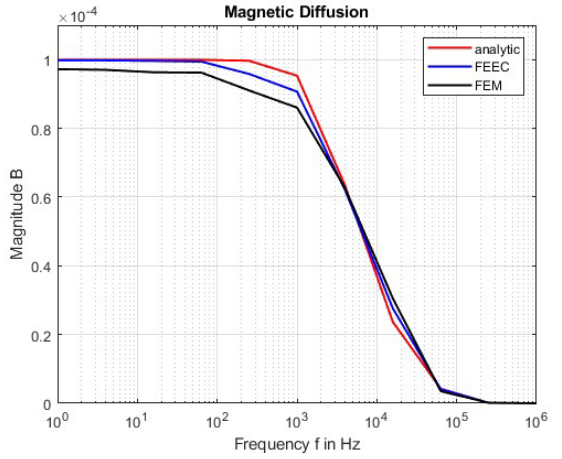

FIGURE 13. Numerical results illustrating the comparison of FEEC with FEM solutions at the radial position $r = 1.1$ mm.

$\gamma = \sqrt{i\omega\mu_0\sigma}$ and defines the frequency dependence of the analytical solution.

Figure 11 illustrates a detailed comparison between the analytical solution and numerical results obtained using DEC and FEEC methods for the specified problem. Since the numerical solution is defined on surfaces, specific values corresponding to the radial position $r = 1.1$ mm were extracted using MATLAB for direct comparison. In Figures 12 and 13, a comparison of the two methods is presented using the finite element method, where the integral equations were described in Section 5. The results show that, particularly at low frequencies, the topology-based approaches, DEC and FEEC, yield higher accuracy than FEM. There are small deviations between the two numerical methods and the analytical solution. These deviations can be attributed to the fact that FEEC used first-order elements, and the use of higher-order elements would likely result in more accurate solutions. In the case of DEC, the observed deviations can be attributed to the mesh generated by MATLAB. These meshes are typically centroid-based rather than circumcentric, which affects the construction of the dual mesh and so the definition of the discrete Hodge star operator. Since DEC relies on circumcentric duality to ensure accurate geometric interpretation, deviations from this assumption may introduce errors in the numerical solution. Despite these factors, the numerical results obtained can still be considered valid within the scope of the study. To our best knowledge, no previous research has reported the use of DEC or FEEC simulations in two-dimensional problems that employ a 2-form formulation which means that there are no available comparative results from other studies that could be used to validate the outcomes of our simulations.

7. CONCLUSION

In this paper, the magnetic diffusion equation was solved in the frequency domain using both DEC and FEEC solvers. A detailed derivation of the differential equation and definition in DEC and FEEC were presented. The definitions of the individual operators were illustrated and explained in detail. The magnetic field was treated as a 2-form within the differential equations and numerical simulations, representing the field on surfaces. Subsequently, the numerical results obtained from both methods were compared with an analytical reference value at a specific point within the geometry. The comparison demonstrated that while DEC offers a simple implementation using triangular elements, FEEC, with its more advanced formulations, yields more accurate results than DEC. Overall, both DEC and FEEC provide valuable numerical alternatives in the field of computational electromagnetics. An interesting extension of this formalism would involve the use of the magnetic field intensity **H**, where a 3D treatment would be required if **H** is to be treated as a 1-form within the framework of exterior calculus. In this context, particularly within FEEC, the incorporation of **H** as a 1-form would necessitate careful consideration of the mass matrix definition, as well as the development of extended formulations for the discrete exterior derivative. These modifications would be crucial for accurately representing the magnetic field in three-dimensional domains and for enhancing

the precision of numerical simulations. Future investigations could include more computational examples with irregular and nonhomogeneous domains. Such studies would provide further insight into the robustness of the proposed approach of both presented methods.

REFERENCES

[1] Butori, F. and E. Luongo, "Mean-field magnetohydrodynamics models as scaling limits of stochastic induction equations," *ArXiv:2406.07206*, 2024.

[2] Jafari, A., E. Vishniac, and V. Vaikundaraman, "Magnetic stochasticity and diffusion," *Physical Review E*, Vol. 100, No. 4, 043205, 2019.

[3] Péron, V., "Asymptotic modelling of a skin effect in magnetic conductors," *ArXiv:2502.07808*, 2025.

[4] Beck, G., S. Imperiale, and P. Joly, "Asymptotic modelling of Skin-effects in coaxial cables," *SN Partial Differential Equations and Applications*, Vol. 1, No. 6, 42, 2020.

[5] Ma, Y. and T. L. Hughes, "Quantum skin hall effect," *Physical Review B*, Vol. 108, No. 10, L100301, 2023.

[6] Cartan, E., "Sur certaines expressions différentielles et le problème de Pfaff," *Annales Scientifiques De l'École Normale Supérieure*, Vol. 16, 239–332, 1899.

[7] Arık, M., A. Baykal, T. Dereli, and T. Tanriverdi, "The exterior calculus of quadratic gravity," *ArXiv:2411.00624*, 2024.

[8] Deschamps, G. A., "Electromagnetics and differential forms," *Proceedings of the IEEE*, Vol. 69, No. 6, 676–696, 1981.

[9] Hirani, A. N., "Discrete exterior calculus," Ph.D. dissertation, California Institute of Technology, Pasadena, CA, 2003.

[10] Ptáčková, L. and L. Velho, "A simple and complete discrete exterior calculus on general polygonal meshes," *Computer Aided Geometric Design*, Vol. 88, 102002, 2021.

[11] Yang, M., H. Fang, D. Chen, X. Du, and F. Wang, "The conformal finite-difference time-domain simulation of GPR wave propagation in complex geoelectric structures," *Geofluids*, Vol. 2020, No. 1, 3069372, 2020.

[12] Lau, P., "Curvilinear finite difference method for three-dimensional potential problems," *Journal of Computational Physics*, Vol. 32, No. 3, 325–344, 1979.

[13] Silvester, P. P. and R. L. Ferrari, *Finite Elements for Electrical Engineers*, Cambridge University Press, Cambridge, 1996.

[14] Brenner, S. and L. Scott, *The Mathematical Theory of Finite Element Methods*, Springer, Berlin, 2008.

[15] Ganesan, S. and L. Tobiska, *Finite Elements: Theory and Algorithms*, Cambridge University Press, Cambridge, 2017.

[16] Tobón, L., J. Chen, and Q. H. Liu, "Spurious solutions in mixed finite element method for Maxwell's equations: Dispersion analysis and new basis functions," *Journal of Computational Physics*, Vol. 230, No. 19, 7300–7310, 2011.

[17] Arnold, D. N., *Finite Element Exterior Calculus*, SIAM, Philadelphia, 2018.

[18] Azerad, P. and M.-L. Hanot, "Numerical solution of the div-curl problem by finite element exterior calculus," *ArXiv:2201.06800*, 2022.

[19] Davidson, P. A., *Introduction to Magnetohydrodynamics*, 2nd ed., Cambridge University Press, Cambridge, 2017.

[20] Goedbloed, J. P., R. Keppens, and S. Poedts, *Advanced Magnetohydrodynamics: with Applications to Laboratory and Astrophysical Plasmas*, Cambridge University Press, Cambridge, 2010.

[21] Leone, M., *Theoretische Elektrotechnik: Elektromagnetische Feldtheorie für Ingenieure*, Springer Vieweg, Berlin, 2021.

[22] Sushch, V., "2D discrete Hodge-Dirac operator on the torus," *Symmetry*, Vol. 14, No. 8, 1556, 2022.

[23] Emam, M. H., *Covariant Physics: From Classical Mechanics to General Relativity and Beyond*, Oxford University Press, Oxford, 2021.

[24] Abraham, R., J. E. Marsden, and T. Ratiu, *Manifolds, Tensor Analysis, and Applications*, 2nd ed., Springer, Berlin, 1988.

[25] Landau, L. D. and E. Lifshitz, *The Classical Theory of Fields: Volume 2*, 4th ed., Butterworth-Heinemann, London, 1980.

[26] Tu, L. W., *An Introduction to Manifolds*, 2nd ed., Springer, Berlin, 2011.

[27] Rousseaux, G., "On the physical meaning of the gauge conditions of Classical Electromagnetism: The hydrodynamics analogue viewpoint," *ArXiv:physics/0511047*, 2005.

[28] Whitney, H., *Geometric Integration Theory*, Dover Publications, New York, 2012.

[29] Zhang, B., D.-Y. Na, D. Jiao, and W. C. Chew, "An A-Φ formulation solver in electromagnetics based on discrete exterior calculus," *IEEE Journal on Multiscale and Multiphysics Computational Techniques*, Vol. 8, 11–21, 2022.

[30] Desbrun, M., A. N. Hirani, M. Leok, and J. E. Marsden, "Discrete exterior calculus," *ArXiv:math/0508341*, 2005.

[31] Moschandreou, T. E., K. Afas, and K. Nguyen, *Theoretical and Computational Fluid Mechanics: Existence, Blow-up, and Discrete Exterior Calculus Algorithms*, 1st ed., Chapman and Hall/CRC, New York, 2024.

[32] Boom, P. D., O. Kosmas, L. Margetts, and A. P. Jivkov, "A geometric formulation of linear elasticity based on discrete exterior calculus," *International Journal of Solids and Structures*, Vol. 236-237, 111345, 2022.

[33] Chen, S. C. and W. C. Chew, "Electromagnetic theory with discrete exterior calculus," *Progress In Electromagnetics Research*, Vol. 159, 59–78, 2017.

[34] Saksa, T., "Comparison of finite element and discrete exterior calculus in computation of time-harmonic wave propagation with controllability," *Journal of Computational and Applied Mathematics*, Vol. 457, 116154, 2025.

[35] Chen, S. C. and W. C. Chew, "Numerical electromagnetic frequency domain analysis with discrete exterior calculus," *Journal of Computational Physics*, Vol. 350, 668–689, 2017.

[36] Gu, D. X. and E. Saucan, *Classical and Discrete Differential Geometry: Theory, Applications and Algorithms*, 1st ed., CRC Press, New York, 2023.

[37] Logg, A., K.-A. Mardal, and G. Wells, *Automated Solution of Differential Equations by the Finite Element Method: The FEniCS Book*, Springer Berlin, Heidelberg, 2012.

[38] Holzinger, S., J. Schöberl, and J. Gerstmayr, "The equations of motion for a rigid body using non-redundant unified local velocity coordinates," *Multibody System Dynamics*, Vol. 48, No. 3, 283–309, 2020.

[39] Dubois, F., I. Greff, and C. Pierre, "Raviart-thomas finite elements of petrov-galerkin type," *ESAIM: Mathematical Modelling and Numerical Analysis (ESAIM: M2AN)*, Vol. 53, No. 5, 1553–1576, 2019.

[40] Hiptmair, R. and J. Xu, "Nodal auxiliary space preconditioning in $H(\mathrm{curl})$ and $H(\mathrm{div})$ spaces," *SIAM Journal on Numerical Analysis*, Vol. 45, No. 6, 2483–2509, 2007.

[41] Stern, A. and E. Zampa, "Multisymplecticity in finite element exterior calculus," *Foundations of Computational Mathematics*, 1–50, 2025.

[42] Sánchez, E. M., M. C. Pinto, Y. Güçlü, and O. Maj, "Time-splitting methods for the cold-plasma model using Finite Element Exterior Calculus," *ArXiv Preprint ArXiv:2501.16991*,

2025.

[43] Jin, J.-M., *The Finite Element Method in Electromagnetics*, John Wiley & Sons, 2015.

[44] Robinson, J. C., *An Introduction to Functional Analysis*, 1st ed., Cambridge University Press, 2020.

[45] Davies, A. J., *The Finite Element Method: An Introduction with Partial Differential Equations*, 2nd ed., Oxford University Press, Oxford, 2011.

[46] Anjam, I. and J. Valdman, "Fast MATLAB assembly of FEM matrices in 2D and 3D: Edge elements," *Applied Mathematics and Computation*, Vol. 267, 252–263, 2015.

[47] Zhang, Q., L. Wang, and Z. Zhang, "H^2(curl)-conforming finite elements in 2 dimensions and applications to the quad-curl problem," *SIAM Journal on Scientific Computing*, Vol. 41, No. 3, A1527–A1547, 2019.

[48] Kalantzis, V., A. Gupta, L. Horesh, T. Nowicki, M. S. Squillante, C. W. Wu, T. Gokmen, and H. Avron, "Solving sparse linear systems with approximate inverse preconditioners on analog devices," in *2021 IEEE High Performance Extreme Computing Conference (HPEC)*, 1–7, Waltham, MA, USA, 2021.

[49] Jia, Z. and W. Kang, "A residual based sparse approximate inverse preconditioning procedure for large sparse linear systems," *Numerical Linear Algebra with Applications*, Vol. 24, No. 2, e2080, 2017.

[50] Barata, J. C. A. and M. S. Hussein, "The Moore-Penrose pseudoinverse: A tutorial review of the theory," *Brazilian Journal of Physics*, Vol. 42, No. 1, 146–165, 2012.